Solar Energy Materials & Solar Cells 259 (2023) 112437

Contents lists available at ScienceDirect

Solar Energy Materials and Solar Cells

journal homepage: www.elsevier.com/locate/solmat

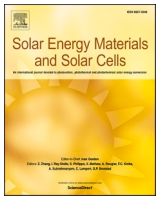

Variability and associated uncertainty in image analysis for soiling characterization in solar energy systems

Greg P. Smestad [a,**], Cody Anderson [b,c], Michael E. Cholette [b], Pavan Fuke [d], Ahmed Amine Hachicha [e,f], Anil Kottantharayil [d], Klemens Ilse [g,h], Mounia Karim [i], Muhammad Zahid Khan [g,h,j], Herbert Merkle [k], David C. Miller [l], Jimmy M. Newkirk [l], Giovanni Picotti [b], Florian Wiesinger [m], Guido Willers [g,h,j], Leonardo Micheli [n,*]

[a] *Sol Ideas Technology Development, San José, CA, USA*
[b] *School of Mechanical, Medical and Process Engineering, Queensland University of Technology, Brisbane, QLD, Australia*
[c] *Dipartimento di Energia, Politecnico di Milano, Milano, Italy*
[d] *Indian Institute of Technology Bombay, Mumbai, India*
[e] *Sustainable and Renewable Energy Engineering Department, University of Sharjah, Sharjah, United Arab Emirates*
[f] *Sustainable Energy and Power System Research Centre, Research Institute for Science and Engineering, University of Sharjah, Sharjah, United Arab Emirates*
[g] *Fraunhofer Center for Silicon Photovoltaics CSP, Halle, Germany*
[h] *Fraunhofer Institute for Microstructure of Materials and Systems IMWS, Halle, Germany*
[i] *University of Derby, Derby, UK*
[j] *Anhalt University of Applied Sciences, Köthen, Anhalt, Germany*
[k] *Cranfield University, Bedford, UK*
[l] *NREL, Golden, CO, USA*
[m] *DLR German Aerospace Center, Institute of Solar Research, Paseo de Almería 73, 2, 04001, Almería, Spain*
[n] *Dept. of Astronautical, Electrical and Energy Engineering (DIAEE), Sapienza University of Rome, Rome, Italy*

ARTICLE INFO

Keywords:
Round Robin
Photovoltaics
Concentrating solar power
Solar energy
Soiling
Microscopy
Image analysis
ImageJ

ABSTRACT

The accumulation of soiling on photovoltaic modules and on the mirrors of concentrating solar power systems causes non-negligible energy losses with economic consequences. These challenges can be mitigated, or even prevented, through appropriate actions if the magnitude of soiling is known. Particle counting analysis is a common procedure to characterize soiling, as it can be easily performed on micrographs of glass coupons or solar devices that have been exposed to the environment. Particle counting does not, however, yield invariant results across institutions. The particle size distribution analysis is affected by the operator of the image analysis software and the methodology utilized. The results of a round-robin study are presented in this work to explore and elucidate the uncertainty related to particle counting and its effect on the characterization of the soiling of glass surfaces used in solar energy conversion systems. An international group of soiling experts analysed the same 8 micrographs using the same open-source ImageJ software package. The variation in the particle analyses results were investigated to identify specimen characteristics with the lowest coefficient of variation (CV) and the least uncertainty among the various operators. The mean particle diameter showed the lowest CV among the investigated characteristics, whereas the number of particles exhibited the largest CV. Additional parameters, such as the fractional area coverage by particles and parameters related to the distribution's shape yielded intermediate CV values. These results can provide insights on the magnitude inter-lab variability and uncertainty for optical and microscope-based soiling monitoring and characterization.

* Corresponding author.
** Corresponding author.
E-mail addresses: inquiries@solideas.com (G.P. Smestad), leonardo.micheli@uniroma1.it (L. Micheli).

https://doi.org/10.1016/j.solmat.2023.112437
Received 10 March 2023; Received in revised form 13 June 2023; Accepted 16 June 2023
Available online 4 July 2023
0927-0248/© 2023 The Authors. Published by Elsevier B.V. This is an open access article under the CC BY-NC-ND license (http://creativecommons.org/licenses/by-nc-nd/4.0/).

1. Introduction

The United Nations Sustainable Development Goals aim to substantially increase the share of renewable energy by 2030 [1]. Photovoltaics (PV), which directly converts solar radiation into electricity, can significantly contribute to the achievement of this goal. Thanks to its decreasing cost and versatility, PV has seen its capacity grow exponentially in the last decade, reaching its first terawatt (TW) in 2022. A recent forecast [2] estimates that PV capacity will be doubled by 2025. Likewise, exponential market growth is expected for concentrating solar power (CSP) power plants [3]. The most common CSP systems power a turbine by heating a fluid through the concentration of sunlight.

However, in parallel to adding new generating capacity, it is also important to maximize the performance of existing installations. This way, one can increase the energy yield of operating solar power plants, minimize their operation and maintenance (O&M) costs, maximize their land- and material-use efficiencies, and lower their energy payback time. One of the main performance issues affecting the energy yield of both PV and CSP plants is soiling. This is due to the accumulation of dust, dirt, and other contaminants on the glass surface of PV modules or on the CSP mirrors [4]. Soiling effectively reduces the intensity of the sunlight and, therefore, the solar energy that can be converted into electricity.

Soiling is reversible and can be typically removed through an appropriate cleaning schedule. In addition, preventive solutions, such as anti-soiling (AS) coatings, can also be used to slow down the soiling accumulation rate, or to facilitate its natural removal by dew or rainfall [5]. However, to be profitable, any soiling mitigation or prevention strategies have to generate revenues higher than their cost [6,7]. Therefore, it is important to plan them according to the severity of the expected losses. This can be done through the installation of soiling monitors in operational PV plants, as recommended in IEC 61724–1 [8]. Soiling monitors can be installed even earlier to estimate the expected cost of soiling and mitigation during the site selection or the system design phases of new solar power plants.

Various approaches have been proposed and are being investigated to monitor soiling losses of fielded PV systems. These include the so-called soiling stations, where the outputs of dirty and clean solar cells are compared. However, the interest for low-cost solutions has been increasing and has led to the development of optical sensors which estimate soiling by characterizing the dust deposited on glass coupons [9,10]. At the fundamental level, there should be a strong correlation between the surface area covered by particulate matter and the optical transmittance of the glass. This has been demonstrated by several groups [10–16] and will be described shortly. It has also been previously shown that the soiling-related performance losses of PV conversion systems typically correlate linearly with the transmission loss of the glass [17]. Valerino et al. [9] utilized both an *in situ* digital microscope outdoors and an optical microscope indoors to monitor the soiling of glass coupons soiled outdoors. The authors used the particle size distribution (PSD) results to estimate the PV losses due to soiling, which compared favourably with a commercial soiling monitoring station in the field. For CSP systems, light is scattered off the front surface of a mirror in the presence of any particles on the glass, and it is then transmitted through it to be reflected off of the silver coating at the back surface. The correlation between the PSD, mirror reflectance and performance has also been reported previously [18]. Given the connection between the presence of dust and the resulting changes in optical properties, there is a need to establish the uncertainty and variability in the characterization of the area coverage and, in general, in the description of the PSD, a precursor to it.

In addition, image-based microscopy and image processing are useful tools for determining realistic dust size and size distribution without assuming a spherical shape. This is in contrast to indirect advanced methods that involve scattered or laser diffracted light, which typically assume a spherical shape [19]. The characterization of dust size and morphology could help in developing the appropriate cleaning method, such as self-cleaning coatings [20,21], and understand the interaction between the particles and the surface of the solar device.

Because of the abovementioned reasons, several authors have investigated the possibility of using image analysis to estimate and monitor the soiling losses. This can be done, for example, by installing an *in situ* digital microscope outdoors, as reported by Figgis et al. [10]. In that work, the authors explored the use of a low-cost device to continuously measure particle deposition and removal on a glass coupon. Through the analysis of particles larger than 10 μm^2, they found a correlation between the surface area coverage and optical transmittance loss. They also found a linear correlation between both parameters and the accumulation per unit area of the glass. Alternatively, glass coupons soiled in the field or in controlled laboratory conditions have been analysed using microscopy. Picotti et al. [18] performed a series of experiments on artificially soiled mirror samples, exploiting various techniques, including: a reflectometer, a spectrophotometer and image analysis of micrographs to identify similarities and differences when adopting image analysis compared to other methods. In 2016, Bahattab et al. [11] reported a linear relationship between surface coverage and the relative loss of optical transmittance. The authors used Arizona test dusts of different grades and found that the correlation was independent of the dust particle size. In the same year, Burton et al. [12] reported a linear correlation between area coverage and transmittance loss, and both were correlated to the mass accumulation as well. An essentially linear relationship, with a negative slope, between the output power for a PV module and mass accumulation per unit area was also observed by Hachicha et al. [16]. Surface coverage, transmittance loss and deposited mass were found to increase at a linear rate (mass/area versus time) by Ilse et al. [13]. Smestad et al. [14] proposed a linear equation to describe the correlation between the broadband transmittance and the area coverage of soiling deposited on coupons installed in seven locations worldwide. A linear correlation between area coverage and transmittance loss was also reported by Einhorn et al. [15], who found the same slope for coupons soiled in Dubai (United Arab Emirates) and Mumbai (India). The authors attributed the result to the similar contribution of inorganic and organic particulate matter to the overall transmittance losses.

Bessa et al. [22] examined many of these experimental correlations, and fit the data to linear equations to compare them. For the area coverage by particles versus broadband (average) relative transmittance, a factor of approximately 3x was found between the smallest and the largest experimental slopes. Therefore, while all the aforementioned works agree that a linear correlation between area coverage and transmittance loss could exist, the slope for this correlation is not consistent. Part of this inconsistency is likely due to the differences in soiling at different locations. The acceptance angle and corresponding transmittance or reflectance may also vary between laboratories and instruments, including those using an integrating sphere. The optical properties of the deposited particles, which in part depend on their chemical composition, are factors that determine the transmission losses of the glass (see, for example, [9]). In addition, because of the size distribution of the deposited particles, soiling losses are more intense in the blue region of the solar spectrum compared to the red-infrared regions [23]. The average soiling loss therefore varies depending on the considered waveband. However, there are also additional factors that must be taken into account. For example, micrographs of particles deposited by soiling have been taken using different microscopes and various magnifications. In addition, they have been analysed through dissimilar image analysis programs and procedures. Understandably, a different approach in any of these steps could produce different results. Particle analysis is affected by both subjective and objective factors, such as: operator, microscope, magnification, lighting, and particle analysis methodology.

This work aims to understand some of the uncertainties that are the result of the applied image analysis, investigating the effects of the

particle characterization procedure on the quantification of soiling. This is accomplished by conducting a round robin among international PV and CSP soiling experts. Eight micrographs were provided to each expert, who separately conducted a particle counting analysis using the same software package. This way, the uncertainty in soiling estimation solely related to the image analysis procedure could be quantified. In addition to the area coverage by the deposited particles, several other parameters derived from microscopy and some reported in previous soiling studies were examined. This way, characteristic soiling parameters most and least affected by the image analysis procedures were identified.

In this work, various image analysis approaches and techniques are compared in order to quantify the differences among them. Indeed, thus far, due to a lack of a standardized methodology, the uncertainty in image analysis has been neglected in soiling-related studies. It should be highlighted that this work does not aim to identify the accuracies of the various methods, but rather to raise awareness on the potential dissimilarities that can be generated by different operators performing an analysis of the same micrographs, even when the same software is employed. The results of this work can provide useful information and insights on optical and microscope-based soiling monitoring and characterization.

2. Methods

2.1. Soiling micrographs

Each expert was provided with the same set of 8 micrographs. These were of glass coupons soiled outdoors in the locations given in Table 1. The coupons were slides made of high-quality Duran soda-lime glass (76 x 26 mm according to ISO 9037–1) from the DWK Life Sciences, LLC. The coupons had a material thickness of 1 +/- 0.05 mm and a hydrolytic class of 3 and were attached to solar modules at each of eight locations in eight different countries with arid regions. These were at or near the Sonoran Desert in the U.S., the Atacama Desert in Chile, the Sahara Desert in Morocco and Algeria, the Great Arabian Desert in Qatar and Jordan, the Simpson Desert in Australia and the arid region of Cape Verde.

A Carl Zeiss Axio A1 microscope with dark field (DF) illumination was used to capture the micrographs. The objective lens was 20x magnification, resulting in a scale 3.156 pixels/μm. The images had a dimension of 1388 pixels x 1040 pixels and were provided in “bmp” format.

2.2. Particle counting analysis

The particle counting was conducted by all participants using ImageJ [27], or Fiji [28]. ImageJ is an open-source image analysis software package developed in Java by the U.S. National Institutes of Health. It was chosen because of two aspects: (i) it is well known among data analysts, and (ii) it was already employed in several soiling studies, briefly reviewed in Table 2. Fiji is an open-source software package for image analysis that is based on the ImageJ software. It bundles the core application of ImageJ with a curated selection of pre-installed plugins.

The experts were asked to set the aforementioned scale and generate a results table containing the areas of all the particles in each micrograph. The experts were instructed to repeat the analysis twice per each micrograph. One set of results was to be produced using ImageJ’s automatic settings for the threshold function. The second set was to be generated by manually setting the threshold values. No other instructions were given.

Thresholding is an image processing method that creates a bitonal (aka binary black and white) image based on setting a threshold value on the pixel intensity of the original image. The analysis can be applied to grayscale as well as to colour images. ImageJ employs thresholds to distinguish if a pixel is a particle or background. Identifying the lower

Table 1
List of the images used in this round robin, along with some characteristics of the locations, calculated from the 2022 data available in NASA MERRA-2 [24,25]. *The corresponding Köppen-Geiger climate classification is given, sourced from* Ref. [26]. *PM_{10} and $PM_{2.5}$ are expressed as average of the hourly measurements in 2022.*

Micrograph No.	Micrograph	Location & Country	Location (latitude [°], longitude [°])	Installation date (No. of days of exposure)	Climate	Annual Avg. Hourly PM_{10} [μg/m^3]	Annual Avg. Hourly $PM_{2.5}$ [μg/m^3]	Rainfall Intensity [mm/year]
1	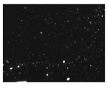	Alice Springs, Australia	−23.76, 133.87	2017-03-06 (3)	Hot Arid Desert (BWh)	23.9	7.8	342
2	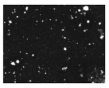	Doha, Qatar	25.32, 51.43	2016-10-16 (1)	Hot Arid Desert (BWh)	351.2	96.9	84
3	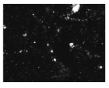	Riverside, USA	33.77, −116.35	2016-11-21 (28)	Hot Arid Desert (BWh)	21.2	9.1	84
4	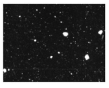	Adrar, Algeria	27.97, −0.18	2017-04-08 (14)	Hot Arid Desert (BWh)	354.1	89.0	4
5	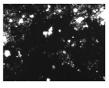	Atacama Desert, Chile	−24.09, −69.92	2017-03-21 (28)	Cold Arid Desert (BWk)	26.7	11.7	15
6	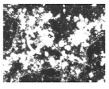	Amman, Jordan	32.02, 35.85	2017-08-01 (28)	Hot Arid Steppe (BSh)	69.5	24.0	195
7	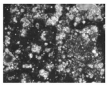	Calhau, Cape Verde	16.86, −24.86	2017-01-06 (28)	Hot Arid Desert (BWh)	100.2	26.1	302
8	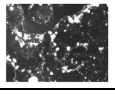	Ben Guerir, Morocco	32.22, −7.92	2017-04-27 (29)	Hot Arid Steppe (BSh)	61.1	19.2	239

Table 2
Review of previous PV and CSP soiling works employing ImageJ showing location, sample information (incl. size and mounting) and analysis parameters.

Reference	Location	Coupon information	ImageJ analysis parameters
[5]	Indoor test	10 × 10 cm^2 artificially soiled glass coupons (uncoated, ARC, ASC)	Surface coverage
[9]	Gandhinagar, India	2.2 × 2.2 cm^2, outdoor mounted glass coupon, monitored with a microscope	Mass loading
[10]	Doha, Qatar	5 × 5 cm^2 outdoor mounted glass coupon, monitored with a microscope	Projected area
[13]	Doha, Qatar	5 × 5 cm^2 outdoor mounted glass coupon	Surface coverage
[14]	Multiple locations	4 × 4 cm^2 outdoor mounted glass coupon	Particle size distribution and surface coverage
[15]	Multiple locations	7.5 × 7.5 cm^2 outdoor mounted glass coupon	Surface coverage, number of particles
[17]	Indoor test	7.62 × 7.62 cm^2 artificially soiled glass coupon	Micrograph processing
[18]	Indoor test	10 × 10 cm^2 artificially soiled low-iron solar glass with silver back coating	Particle size distribution and diameter
[29]	Indoor and Outdoor (Atacama Desert, Chile)	10 × 10 cm^2, tilt angle 20°	Surface coverage
[30]	Atacama Desert, Chile	6.5 × 5.8 cm^2 outdoor mounted glass coupons	Shape factor and particle size distribution.
[31]	Doha, Qatar	5 × 5 cm^2 outdoor mounted glass coupon, monitored with a microscope	Mass loading and particle diameter
[32]	Alentejo, Portugal	11 × 9 cm^2 glass coupon at various inclinations (using glass "tree" mount)	Particle diameter
[33]	Doha, Qatar	5 × 5 cm^2 outdoor mounted glass coupon, monitored with a microscope	Surface coverage
[34]	Howrah, India	5 × 5 cm^2 outdoor 8 different tilt angles	Particle size distribution and diameter
[35]	Indoor test	10 × 10 cm^2 artificially soiled glass coupons; volcanic dust	Particle size distribution and diameters

and upper threshold values (via lower and upper limits) is therefore needed to discern features of interest (i.e., particles in this case) against the background.

The automatic threshold capability of ImageJ was used to automatically identify the upper and lower threshold values, based on additional available settings. The use of automatic thresholding in this study could be used to assess any intrinsic variation from the ImageJ software itself. A second set of results was generated by each expert (operator) by visually setting the upper and lower threshold values (via sliders). This way, it was possible to evaluate the differences between the automatic and the manual thresholding procedures, and to investigate any dissimilarity in the results due to the expert's own subjective perspective.

The ImageJ operators have been labelled using consecutive numbers, from 1 to 11 (O1, O2, O3, …, O11) and the primary distinguishing features of each are summarized in Table 3. As can be seen, there were a diversity of conditions and settings utilized. For the automatic approach to the thresholding, operators O4 through O11 set the auto threshold to the so called "Default Dark" condition (refer to Table 3). This is accomplished by the sequence: Image 〉 Adjust 〉 Threshold from the menu and then selecting Default, Dark background and "Auto." There are several methods to set the threshold automatically. These include the aforementioned Default Dark, as well as Otsu dark, Triangle and several others. The operators were instructed to employ an auto threshold method, as well as a manual method. The ramifications of this will be discussed in Section 3.4.

Methods employed by operators O1, O2 and O6 ran the analysis after ensuring that the image was converted to an 8-bit greyscale. It should be noted that all of the micrographs of the study were 8-bit. Operators O4, O6 and O7 converted the image using a "Mask". This created a black and white image based on the current threshold settings. ImageJ can be set to deal with white particles on a black background or black particles on a white background. The default condition in ImageJ is that the background colour is white and the foreground colour is black. Operators O4, O6 and O10 selected black particles on a white background. Operator O7 set this option so that there was a black background with the foreground colour as white, as in a darkfield image.

"Analyze Particles exclude" in Table 3 refers to excluding particles that intersect with the boundaries of the micrograph. The term "include" (which is the default in the menu for Analyze Particles) allows ImageJ to find the extent of the particle by tracing the outer edge and filling within. This includes interior holes as part of the larger particle. All the methodologies were recorded using the macro-recorder function in ImageJ and are available in the data archive (Mendeley) or upon request.

2.3. Comparison

The analysis was conducted by comparing the results obtained by the experts for the same set of 8 micrographs. The assessment of the different methodologies was conducted by calculating the parameters given in Table 4. These are either statistical parameters, typically employed to characterize probability distributions, or soiling-related variables. The first group includes the mean, median, mode particle size, the particle size distribution's skewness and kurtosis, the number of particles counted, and percentage of surface area coverage by the particles (i.e., ratio of the sum of the particle areas to the micrograph surface area). When diameters are reported, these are "equivalent diameters", calculated from the projected area returned by ImageJ and assuming the particles were spherical. The second category includes L and L_{slope}, two parameters used in a previous investigation [14] to describe the PV soiling particle size distribution and explained shortly. It should be re-emphasized that the aim of this work is not the evaluation of the effectiveness or utility of the various parameters in soiling characterization. Rather, this work only aims to evaluate their robustness to the different image analysis approaches.

There are international standards that are useful in the characterization of deposited dust, soil and particulate matter, as well as their analysis by image analysis. These include ISO 14688–1 that describes the identification and classification of soils in terms of sizes. ISO 13322-1 describes image analysis [36] and ISO 9276 parts 1 and 2 focus on the representation of results [37,38]. The latter standard utilizes histograms to visualize the particle size distribution (PSD). A histogram is an effective graphical technique for showing both the skewness and kurtosis of a data set, as shown in Fig. 1. Skewness and kurtosis are parameters typically used in the analysis of distributions [39]. The skewness measures the lack of symmetry in a distribution (and therefore in its histogram). It is zero if the histogram is symmetrical. A negative skewness means that the histogram has a longer tail on the left side, and, therefore, the mean is lower than the median. On other hand, a positive skewness means that the histogram is right-tailed and that the mean is greater than the median. The kurtosis measures whether the data in the histogram is heavy-tailed or light-tailed relative to a normal distribution. Positive values of kurtosis indicate that distribution is peaked and

Table 3
Summary of the test method used by the eleven indicated ImageJ operators for the automatic approach. The use of the most recurring functions is also highlighted. A representative flow chart for methods O5, O8, O9, O11 can be found in the Supplementary Information (Figure S1).

Method	Distinguishing features	Auto Threshold: Default Dark	Black Background	Mask	Analyze Particles exclude	8-bit	Other
O1	Create two masks: 1) large particles and 2) a difference of Gaussian curves with triangle threshold. The analysis was run after converting the image to binary (8-bit greyscale).			✓	✓	✓	Otsu Dark, Triangle Dark
O2	Create three masks: 1) large particles, 2) a difference of Gaussian curves with triangle threshold, and 3) segmented particle maxima search. The analysis was run after converting the image to binary (8-bit greyscale).			✓	✓	✓	Otsu Dark, Triangle Dark
O3	Run the auto threshold using the "Default white" method using Auto Threshold. Particles are specified to be the brighter components of the image.				✓		
O4	Run the default auto threshold method, thresholding the darker pixels of the image. Ensure that the background of the thresholded image is white. Create a black and white image based on the threshold settings.	✓	FALSE	✓			
O5	Run the default auto threshold method, thresholding the darker pixels of the image.	✓					
O6	The analysis was run after converting the image to binary (8-bit greyscale). Sharpen, enhance and adjust contrast. Run the default auto threshold method, thresholding the darker pixels of the image. Convert the image to black and white based on the threshold settings.	✓	FALSE	✓	✓	✓	Enhance Contrast
O7	Run the default auto threshold method, thresholding the darker pixels of the image. Background colour is black and the foreground colour is white. Convert the image to black and white based on the threshold settings.	✓	TRUE	✓			display include
O8	Run the default auto threshold method, thresholding the darker pixels of the image.	✓					
O9	Run the default auto threshold method, thresholding the darker pixels of the image.	✓					display clear
O10	Run the default auto threshold method, thresholding the darker pixels of the image. Ensure that the background of the thresholded image is white.	✓	FALSE				
O11	Run the default auto threshold method, thresholding the darker pixels of the image.	✓					

Table 4
Parameters used in the comparative analysis.

Parameter	Symbol	Description	Unit
Area coverage	f	Fraction of micrograph area covered by particles	–
Count	N	Number of counted particles	–
Mean	D (mean)	Average diameter of the counted particles	μm
Median	D (median)	Median value of the diameters of the counted particles	μm
Mode	D (mode)	Most recurrent diameter in each results table	μm
Skewness	Skew	Measure of the asymmetricity of the distribution	–
Kurtosis	Kurt	Difference in tails relative to a normal distribution	–
Cleanliness Level	L	Extrapolated value expressing the largest particle	μm
Slope (for Cleanliness)	L_{slope}	Slope of the log-log^2 particle size distribution	–

possesses thick (heavy) tails.

In addition to particles' size-specific parameters, two other factors recently suggested for outdoor soiling [14] have also been considered. These are the cleanliness level, L, and a parameter named L_{slope}. The cleanliness level is a parameter originally proposed in IEST-STD-CC 1246E to describe the cumulative distribution of diameters of deposited particles or contaminants [40]. The IEST document has been used as an industry standard for cleanrooms for optics and spacecraft. For the standard, the lognormal cumulative distribution was selected and approximated by a log-log^2 equation. This means that the cumulative distribution of particles per unit area can be described as:

$$N(D) = \frac{10^{L_{slope} \bullet \left[(\log_{10} L)^2 - (\log_{10} D)^2\right]}}{0.1\ m^2} \quad (1)$$

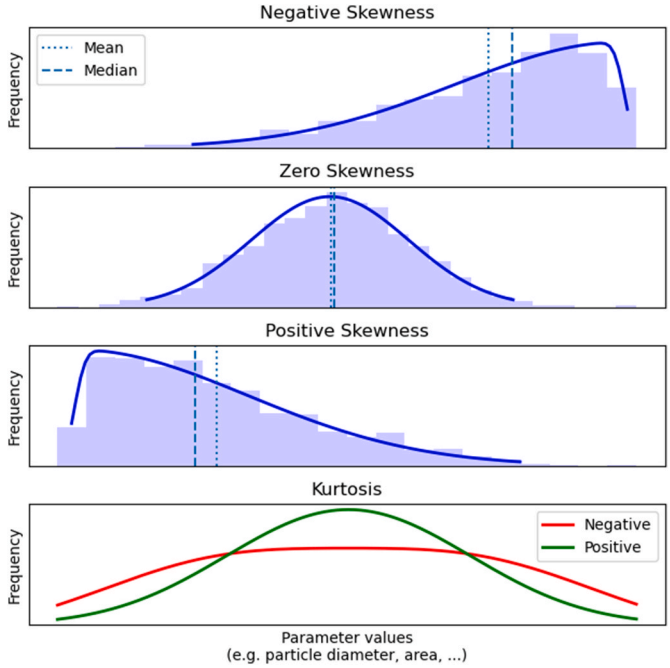

Fig. 1. Examples of distributions with negative and positive signs for skewness and kurtosis.

where N(D) is the number of particles per unit of area having a diameter between D and L (both in micrometers). L therefore is a measure of the maximum diameter in the distribution and corresponds to the value at which the log-log^2 curve intercepts the y-axis. L_{slope} represents the change in the logarithm of the cumulative number of particles at a given

effective diameter versus the change in the square of the logarithm of the corresponding effective diameter.

Smestad et al. [14] found that the particles deposited via outdoor soiling also follow the same size distribution equation, especially for low-to-moderate soiling levels. The particle size distribution for soiling on glass coupons fits this standard with a typical L value lying within the range 500–1200 μm. While the accepted slope for the log-log^2 plot is 0.926, variation around that value is possible. The particle size distribution of airborne- and surface accumulated-matter typically follows logarithmic distribution, e.g., the Krumbein phi scale [41]. The PSD of contaminated surfaces can be compared to the local soil, a primary source of PM_{10} matter, and a standardized taxonomy is given in ISO 14688–1 [42].

The distribution of each parameter given in Table 4 was studied through the coefficient of variation, CV. This is a statistical index expressing the relative dispersion of data points around the mean. It is calculated as the ratio of the standard deviation to the mean. The larger its value, the larger the distribution of values calculated by the experts. Lower values, on the other hand, prove better reproducibility (or lower variance) in the calculation of the given parameter.

The international standard ASTM E691 describes a reproducibility index, R, for round robins between different laboratories [43]. This standard also utilizes the repeatability, which describes the variation in the successive measurements made by the same operator under the same conditions. However, the present work does not account for the intra-lab variability (repeatability), as ImageJ produces the same results if the same scripts used here are applied multiple times. Therefore, in this case, the reproducibility is reduced to 2.8 times the standard deviation between labs for the measurements of a particular parameter. When parameters with different magnitudes are compared, the reproducibility calculation returns values that are dependent on both the variability of the results and the magnitude of each parameter. In other words, parameters with larger magnitudes, such as L (whose values typically range in between 700 and 1300 μm), are likely to possess larger R values compared to parameters with smaller magnitudes, such as the mean diameter (typically expressed in μm, with mean values on the order <10 μm). For these reasons, the use of the coefficient of variation (a standard deviation divided by the mean) is favoured in the present work over R, as it provides a "normalised" value that makes it possible to compare various parameters with different magnitudes.

However, other aspects of the ASTM E691 standard were used. In a preliminary step, the Mandel's h test [43] has been employed to identify outliers among the participants. The h value is a difference between a measurement and a mean value, both divided by a standard deviation. In particular, results from operators returning Mendel's h values consistently outside of a critical value were censored.

The analysis was conducted using a custom program written in Python 3.7. Specialised functions were provided in the SciPy library [44]. For example, a curve fit was performed using the *curve_fit* function.

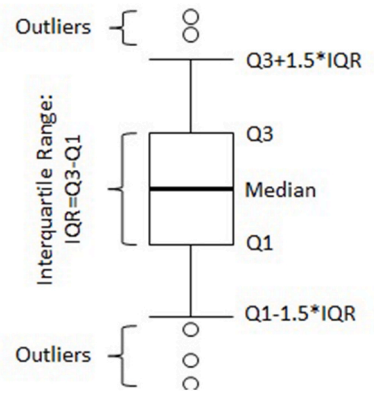

Fig. 2. Parts of a boxplot. In some cases, outliers are not always shown.

Boxplots are used for visualisation of some of the results (Fig. 2). These consist of: (i) a box spanning from the first to the third quartiles (Q1 and Q3), and (ii) "whiskers" (vertical lines) that are 1.5 times the interquartile range long (Q3-Q1). The black line in the box shows the median value.

3. Results and discussion

3.1. Outliers

Of all the participants, O6's results were often identified as outliers by the Mandel's h test (Fig. 3). When D (mean) is calculated, Mendel's h for O6 is outside of the threshold in 100% of the cases for manual thresholding and in 87.5% for automatic thresholding. In the calculation of N, these percentages decreased to 62.5%. No other method has such high occurrences. Operators O1, O2, O4 and O10 occasionally have Mendel's h values higher than the threshold, but for no more than 25% of the micrographs.

For this reason, results from O6 have not been considered in the rest of the analysis. This method counted 1 to 8 times more particles on average than the other methods. These were between 50 and 60% smaller on average compared to the other datasets. The results were likely due to the application of the sharpen, enhance, and contrast features available in under the "Process" menu in ImageJ (see Table 3).

3.2. Particle size distribution

A preliminary visual inspection of the particle size distributions was conducted. The PSD of the soiled glass coupons followed a similar shape, depicted as a histogram for a representative micrograph in Fig. 4. For this micrograph, the mean and median value of the diameter is 2.4 μm and 1.4 μm, respectively, when averaged over all ImageJ operators. For all micrographs, the particle size was found to be dominated by the smallest diameters. The micrographs exhibit a median diameter between 0.88 μm and 1.86 μm, whereas the mode diameter has a value lower than 2 μm. All the PSD histograms can be found in the Supplemental Information. The value for the mean diameter is somewhat smaller than the average of 16 μm reported from a survey of the literature for soiling collected in the field at many sites worldwide [45]. This can be explained by three factors: (1) only 4 of those studies were conducted by using light microscopy, (2) as found in a previous study [14] PSD results can be affected by the magnification factor, and (3) the present values are for the particle number distribution density, rather than the particle equivalent surface area or volume distribution density [36–38].

The dominance of small particles is not surprising, as it was already reported in previous works. For example, this is the same behaviour observed by Smestad et al. [14] for a soiling study at seven locations world-wide. This has implications for the type of light scattering from the deposited particles – it will be dominated by Mie scattering [46]. However, it should be acknowledged that both in the present and in the prior work [14], soiled coupons have been analysed in locations different from where they were mounted. Because of this, some particles might have fallen off during handling and transportation. Despite that, as also shown in Table 2, the use of glass coupons for soiling studies is a common practice [47–49]. Moreover, it should be highlighted that the aim of the present work is the analysis of the particles deposited on glass coupons, not the characterization of soiling at different sites and its correlation to the local conditions.

The maximum diameter range is from 11.03 μm to 309.59 μm. There is a long tail in the PSD out to larger particle sizes (see Fig. 4). The right-tailing of the distributions is also confirmed by the skewness that will shortly be described further. This, indeed, is always positive in the given dataset, reaching an average value, over all the operators, of 7.4% for the PSD of Fig. 4. The corresponding average kurtosis is 79%.

The most notable difference between the automatic and manual thresholding is in the number of particles counted. As will shortly be

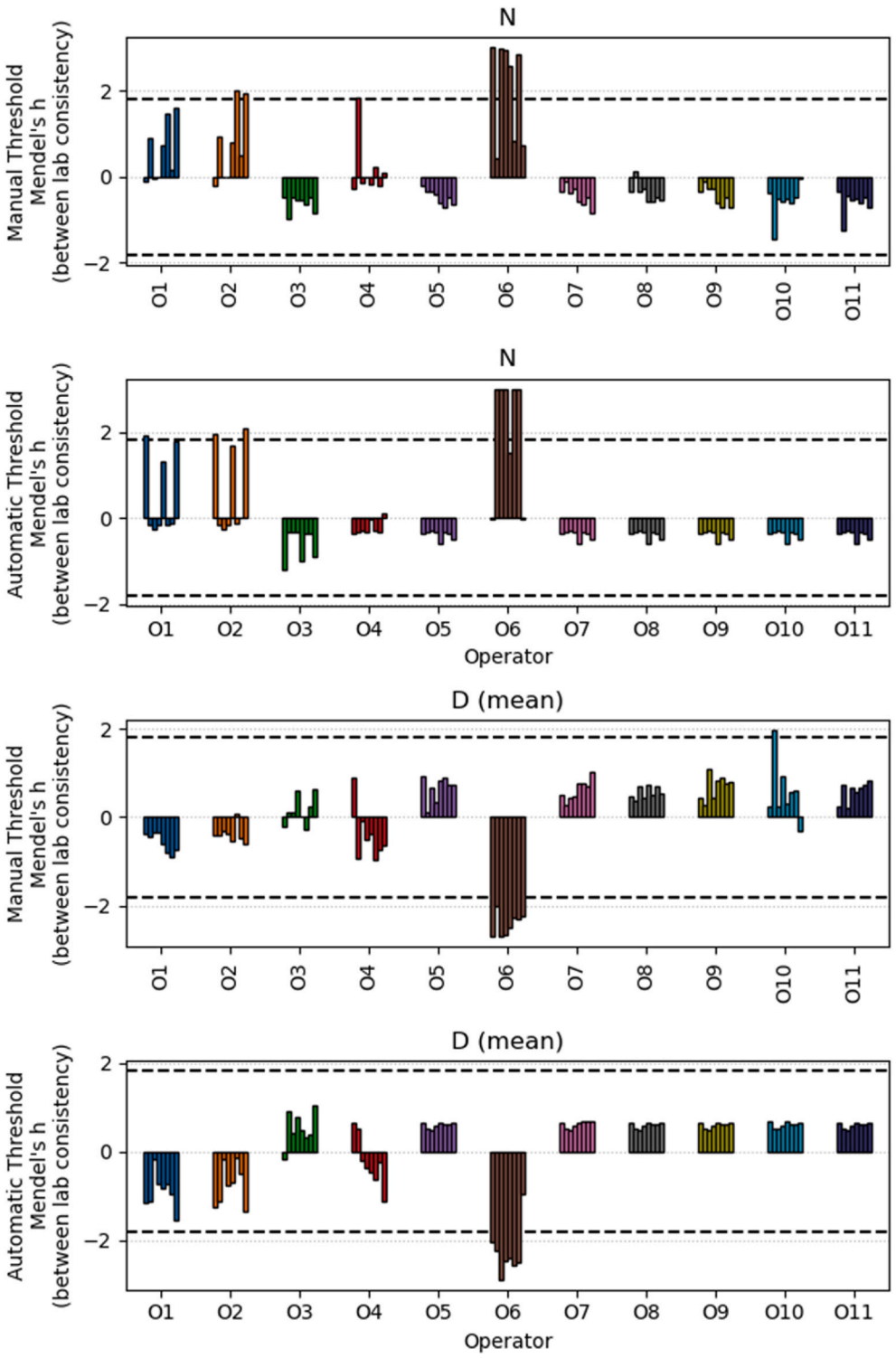

Fig. 3. Results of Mendel's h test for N and D (mean) and for both automatic and manual thresholds for each operator (x-axis).

illustrated in section 3.5, manual thresholding is indeed found to lead to a larger number of counted particles in the majority of cases. Specifically, using manual thresholds resulted in approximately 19% more particles counted compared to the automatic thresholding approaches. A further discussion on the differences between thresholding methods can be found in the sections that follow.

Fig. 5 represents the same PSD, but plotted on a log-log scale as a continuous function using the aforementioned pixel size (3.156 pixels/μm) and its multiples. In Fig. 5, one can see that a cumulative number of particles on the order of 1000 is obtained by integrating the curve from 0 to 1 μm, the bin size used for the histogram of Fig. 4. As mentioned previously, it has been shown [14] that a description of the cumulative particle size distribution of dust particulates deposited outdoors can be made for lightly-soiled coupons using IEST-STD-CC 1246E [40]. According to this standard, the particle size distribution can be described by the two aforementioned parameters, L and L_{slope}. Such an analysis for each micrograph is found in the Supplemental Information for both automatic and manual thresholds.

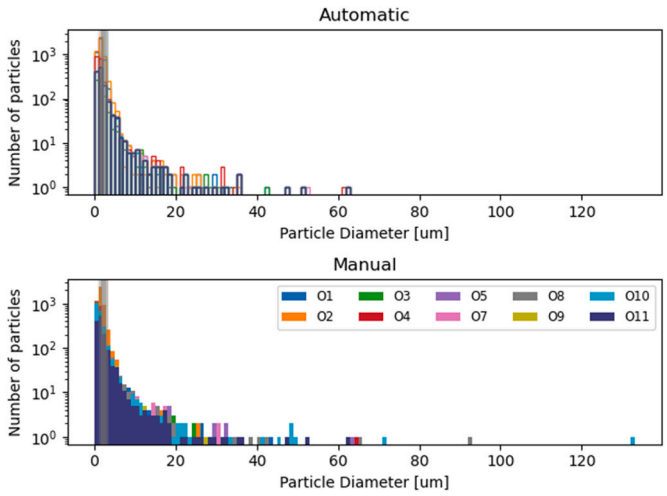

Fig. 4. Representative particle size distributions for micrograph 8 soiled in Morocco. The results are shown for various operators (indicated by the color) using ImageJ for the automatic (top) and manual (bottom) settings. The bin size is one micron. The vertical shaded areas show the mean diameter returned by each operator. Additional PSD histograms, two for each micrograph, can be found in the Supplemental Information.

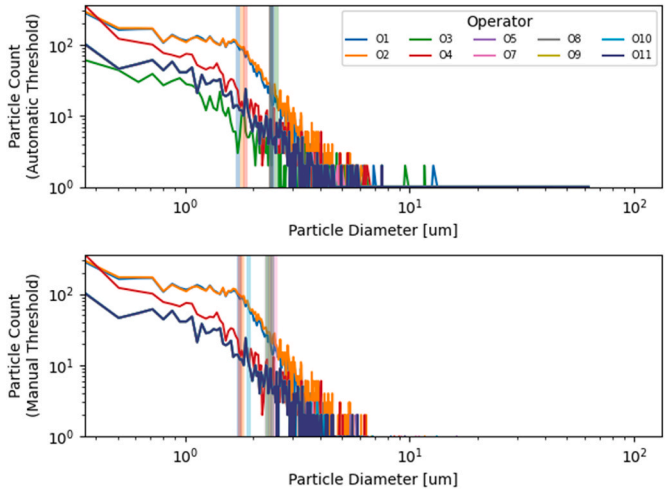

Fig. 5. Log-log distributions of particle size for micrograph 8 soiled in Morocco. The results are shown for various operators (indicated by the color) using ImageJ for the automatic (top) and manual (bottom) settings. The vertical bars show the mean diameter returned by each operator.

3.3. Area coverage and sensitivity analysis of the parameters

The coupons utilized in the present analyses have been exposed to the outdoor conditions at different locations worldwide for periods of 1–29 days (see Table 1). After exposure, the coupons were shipped to Fraunhofer CSP, in Germany, for the microscopy analysis. The variety of exposure locations and timings allowed us to investigate different types and amounts of soiling. This is, in part, documented by the distribution of fractional area (f) coverage values measured by each operator, as shown in Fig. 6. These went from approximately 1% (micrograph 1), up to approximately 40% (micrograph 6), with the highest accumulations found after a 4-week exposure in Morocco (For the correspondence between micrograph number and location, please refer to Table 1.). One should note that the bars in the histogram of Fig. 6 are filled to indicate the manual threshold approach and are unfilled for the automatic threshold approach.

The combined results for all the operators, grouped by parameter, are shown in the boxplots of Fig. 7, summarizing the sensitivity analysis. The upper plot shows the coefficients of variation (CV) for each parameter. The middle plot displays the full extent of the returned deviation from average. The bottom plot reproduces the same results as the middle one, but it is magnified to limit the y-axis to a −100 to +100% range and does not show the results for O1 and O2. For the middle and bottom plots, the results are distinguished by operator indicated by the color code in the legend.

To create the top plot for the CV, the values for all of the parameters (shown in Table 4) for a specific micrograph were tabulated for each of the 10 operators. There were thus 8 tables, one for each micrograph. A mean and standard deviation was obtained for each parameter. Then, a coefficient of variation was calculated as the ratio of the mean to the standard deviation. Another table was then formulated that gave the CV values for the parameters versus the eight micrographs. For example, for micrograph 8 and the parameter f, the CV is 13.4%, but the median for f across all micrographs is 34.8% for the automatic threshold. It is the median value for each parameter across the eight micrographs that is plotted in Fig. 7 as a box plot, as is outlined in Fig. 2. A similar procedure was used for the deviation in average value in Fig. 7. The plots therefore illustrate the variation, or spread, of the CV and the deviation from average for the eight micrographs.

The mean, median and mode diameters, L and L_{slope} are the parameters that are less affected by changes in human operators, achieving median coefficients of variation lower than 20%. The median value for the coefficient of variation from Fig. 7 is approximately 15% for the mean particle diameter, and 8–9% for the median and mode diameters. The skewness and kurtosis are much higher, at 23% and 50%, respectively, while the total number of particles counted, N, returned the highest variability value at 82%. The fractional area coverage utilized by many previous soiling characterization studies [10–15] produced a value of 35%, while, for the cleanliness standard, 15% and 17% were obtained for L and L_{slope}, respectively.

The low coefficients of variation for the diameter metrics can be explained by the aforementioned dominance of small particles in all the measurements. Indeed, as stated in section 3.2, all of the methods returned mean and median diameters between 0.88 μm and 1.86 μm. The value of L is correlated to the largest measured diameter, and computed taking into account the whole particle size distribution; for this reason, the coefficient of variation for L is similar to that of the particle size, D. On the other hand, the number of particles is the parameter that is the most affected by choices made by human operators. The fractional area coverage, f, is intermediate in terms of the coefficient of variation.

It can be seen from Fig. 7 that operators O1 and O2 returned results furthest from the average. These methods indeed tend to report the highest number of particles, especially when an automatic model is employed (deviation from average values was between 100% and 200%). The larger number of smaller particles also impacts the estimation of L and L_{slope}, both higher compared to the other methods, which behave consistently. Overall, O3 tends to return lower values for particle number and area coverage, whereas O1 and O2 typically yield the highest values. The outputs of the other methods are quite consistent. If O1 and O2 are removed and the y-axis re-scaled (as in the lower plot of Fig. 7), it is found that O3 and O4 are the methods returning the results most different from O5–O11, particularly for skewness, kurtosis, particle number and area coverage. From Table 3, one sees that O3 utilized the Auto Threshold feature in ImageJ and the setting "white." This is accomplished via the menu sequence: Image ⟩ Adjust ⟩ Auto Threshold, rather than the sequence employed by O4–O11 (Image ⟩ Adjust ⟩ Threshold, and then Dark and Auto). Operators O1 and O2 utilized another automatic threshold sequence (Image ⟩ Adjust ⟩ Threshold, and then Otsu Dark or Triangle Dark) and a sophisticated sequence of masks to binarize the image using the threshold values.

It should be noted that in view of a lack of a recognized reference micrograph, it is not possible at the moment to identify the accuracy of

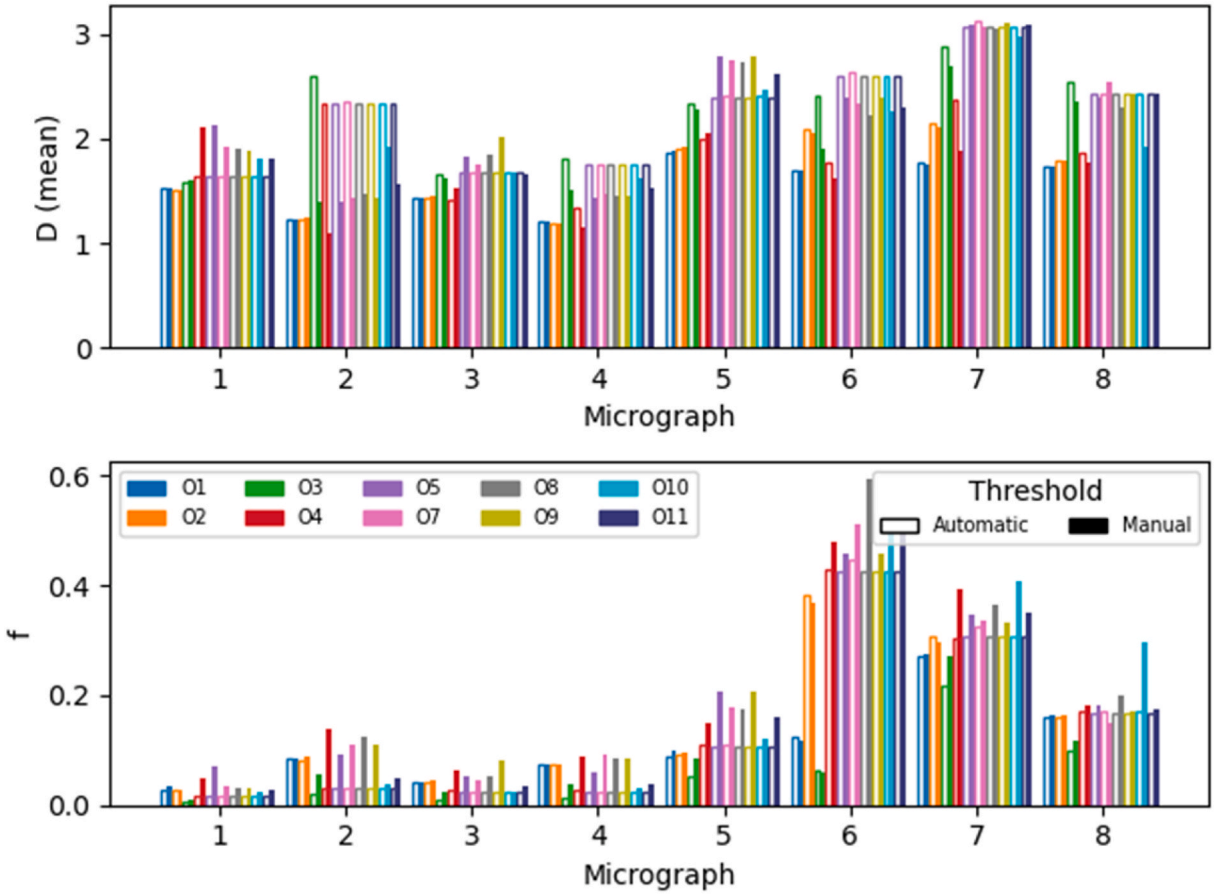

Fig. 6. Mean diameter and fractional area coverage, f, in the present analysis, for the indicated micrograph. The results are shown for various operators (indicated by the color) using ImageJ for automatic and manual settings. The bars are filled to indicate when the manual threshold approach was used and are unfilled for the automatic approach.

the methods (i.e. the difference between the estimated and the correct/true values). The aim of this work is indeed only to evaluate the magnitude of the uncertainty among the various image analysis methods. For this reason, methods such as those labelled as O1–O3 should not be considered less accurate or incorrect. Indeed, these only provide a measure of how different the results can be when they are obtained by the same software for the same micrograph. Additional studies will be needed to evaluate the error produced by the various methods.

The median coefficient of variation of 35% for the fractional area coverage mentioned above can be broken down in terms of the various micrographs. For this, each micrograph is considered as a unique specimen. Both the deposited materials (i.e., the composition of the particles), the characteristics of the particles (i.e., shape and size distribution) and the resulting light scattering will be unique to a location, and therefore to each micrograph described in Table 1. Table 5 shows the micrograph-specific results for the fractional area coverage, f. In Fig. 7, these results are averaged over both the various operators, as well as the variation over the micrographs. Here, we can differentiate the results of the study in terms of the coefficient of variation, CV, and several other commonly used statistical parameters [50]. We can do this in part to determine what error bars should be reported with the mean value $\bar{f}$ of the area coverage for a particular micrograph, and for the study as a whole. For each of the eight darkfield micrographs, there is the mean, a standard deviation (s.d.) and the coefficient of variation (s.d./mean). Also given is the standard error of the mean (s.e.m.) and an approximate 95% confidence interval. The reproducibility, R, is calculated from a consideration of ASTM E691 [43].

The first thing to point out from Table 5 is that not all micrographs have the same CV values. Some exhibit worse variance between the operators than others. Using micrograph 8 again as an example, we can make some recommendations for the reporting of the results of soiling studies based on ImageJ analyses of micrographs. From, the mean value of $\bar{f}$ (0.16) for this micrograph and its standard deviation of 0.02, it is quite reasonable to report the result, averaged over the operators, as $\bar{f} = 0.16 \pm 0.04$. For an assumed approximately normal distribution for the results obtained by the operators for a parameter in Table 4, 95% of the returned values fall within ±2 s.d. This reflects the variation of our round-robin data and not the error in the measurement. Error bars based on the s.d. estimate the spread for the larger population and are therefore useful as predictors of the range of new results if the round robin was repeated. For population that is not approximately normal, the spread is easier to interpret using the interquartile range concepts outlined in Fig. 2.

The round-robin data results are themselves a sample, in particular using 11 labs out of a multitude of many more that could have been used. We have not necessarily measured the whole population and its variation. If we had involved 20 labs (operators), we would not have obtained exactly the same results. We have excluded the results from one operator (O6), so that the number of labs is 10 (let p = 10). The s.e.m. error bars decrease as more measurements are performed (s.e.m. = s.d./$\sqrt{p}$). Error bars based on the s.e.m. reflect the uncertainty in the mean and its dependency on the sample size, p. So, from Table 5, we can also report $\bar{f} = 0.16 \pm 0.007$.

The 95% confidence interval, CI, is approximately given by 95% CI = 2 x s.e.m. This is an interval estimate that indicates the reliability of a measurement. It would capture the population mean 95% of the time.

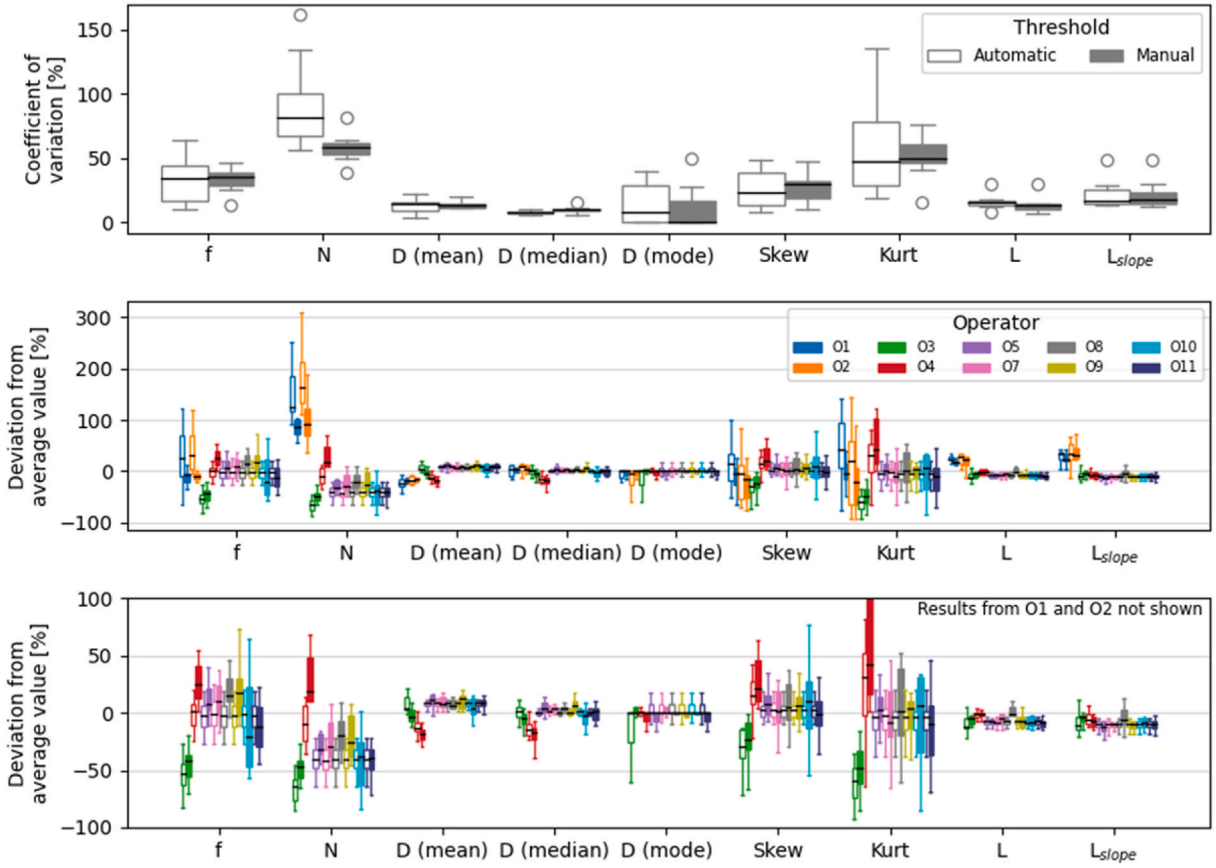

Fig. 7. Coefficients of variation and deviation from average value for the investigated parameters for micrographs 1 to 8 grouped by investigated parameter. The bottom plot does not display the results of O1 and O2 and provides a more limited range to distinguish the deviation from average. The nomenclature used in the image is shown in Table 4.

Table 5
Micrograph-specific data for the automatic threshold setting portion of the ImageJ round robin and the parameter f, the fractional area coverage by the particles deposited by soiling. The mean, standard deviation, coefficient of variance and standard error of the mean are tabulated along with a 95% confidence interval and the reproducibility value, R, value from a consideration of ASTM E691 [43]. The results are summarized for all 10 operators (and exclude O6).

Micrograph	$\bar{f}$	s.d.	CV	s.e.m.	95% CI	R
1	0.0169	0.00584	34.6	0.00185	0.00369	0.0164
2	0.0401	0.02300	57.5	0.00729	0.01460	0.0645
3	0.0274	0.00956	35.0	0.00304	0.00607	0.0269
4	0.0332	0.02136	64.3	0.00675	0.01350	0.0598
5	0.0993	0.01780	18.0	0.00564	0.01130	0.0500
6	0.358	0.14110	39.4	0.04460	0.08930	0.3950
7	0.296	0.03121	10.5	0.00990	0.01970	0.0874
8	0.160	0.02150	13.4	0.00680	0.01360	0.0602

For our study and micrograph 8, considering this confidence interval would yield $\bar{f} = 0.16 \pm 0.014$.

Finally, there is R defined in ASTM E691 as, "the value below which the absolute difference between two test results obtained under reproducibility conditions may be expected to occur with a probability of approximately 0.95 (95%)". Reproducibility conditions refer to, "conditions where test results are obtained with the same method on [nominally] identical test items in different laboratories with different operators using different equipment". Specifically, there is a 95% probability that two test results will differ by not more than R if they are obtained from analyses of nominally identical micrographs conducted by different operators using ImageJ. Since only one replicate from each field specimen was analysed at each lab (n=1), the equations of the E691 standard simplify and R = 2.8 s.d. For micrograph 8, we can thus report $\bar{f} = 0.16 \pm 0.06$, quite a high uncertainty.

These results indicate quite a bit of variability when all the operators, except for O6, are included. The conclusion from this is that when arbitrarily given the task of applying an auto threshold in the use of ImageJ for soiling studies, one should expect a large uncertainty. Caution must therefore be exercised in the interpretation and extension of the results of the prior studies given in Table 2.

If, however, one examines a subset of the operators where the default settings were utilized for thresholding, another recommendation can be made. If one also omits O1–O3 (referring to Table 3), the maximum values across all micrographs for the statistical parameters reported in Table 6 are instead approximately: 0.008 for the s.d.; 0.003 for the s.e.m.; 0.006 for the 95% CI, and a maximum coefficient of variation of 4.2. An R value less than approximately 10% of f is found for that sub-set of eight operators. Clearly, these are values that would allow for meaningful comparisons, those with more precision, to be made in soiling research or estimation of energy production. These results, and the result of trials in which the ImageJ analysis was carried out several times on the same micrograph using the methods given in Table 3, strongly suggest that ImageJ does not intrinsically induce a stochastic variation on its own (For details, refer to the Supplemental Information and Mendeley data archive).

3.4. Thresholding and exclusion approach

Fig. 8 shows the results in terms of both number of particles and threshold level for each micrograph. The corresponding plots for the area coverage and D (mean) for each micrograph can be found in Fig. 6.

Table 6
Micrograph-specific data for the automatic threshold setting portion of the ImageJ round robin and the parameter f, the fractional area coverage by the particles deposited by soiling. The mean, standard deviation, coefficient of variance and standard error of the mean are tabulated along with a 95% confidence interval and the reproducibility value, R, value from a consideration of ASTM E691 [43]. Only the results from O4–O12 were considered (excluding O1–O3 and O6).

Micrograph	$\bar{f}$	s.d.	CV	s.e.m.	95% CI	R
1	0.0156	2.00E-05	0.128	7.56E-06	1.51E-05	5.60E-05
2	0.0304	0.000187	0.614	7.05E-05	0.000141	0.000522
3	0.0256	0.000978	3.820	0.000370	0.000739	0.002740
4	0.0246	0.001040	4.230	0.000393	0.000787	0.002910
5	0.1080	0.000333	0.308	0.000126	0.000252	0.000933
6	0.4300	0.007700	1.790	0.002910	0.005820	0.021600
7	0.3100	0.007930	2.560	0.003000	0.005990	0.022200
8	0.1700	0.000993	0.586	0.000375	0.000751	0.002780

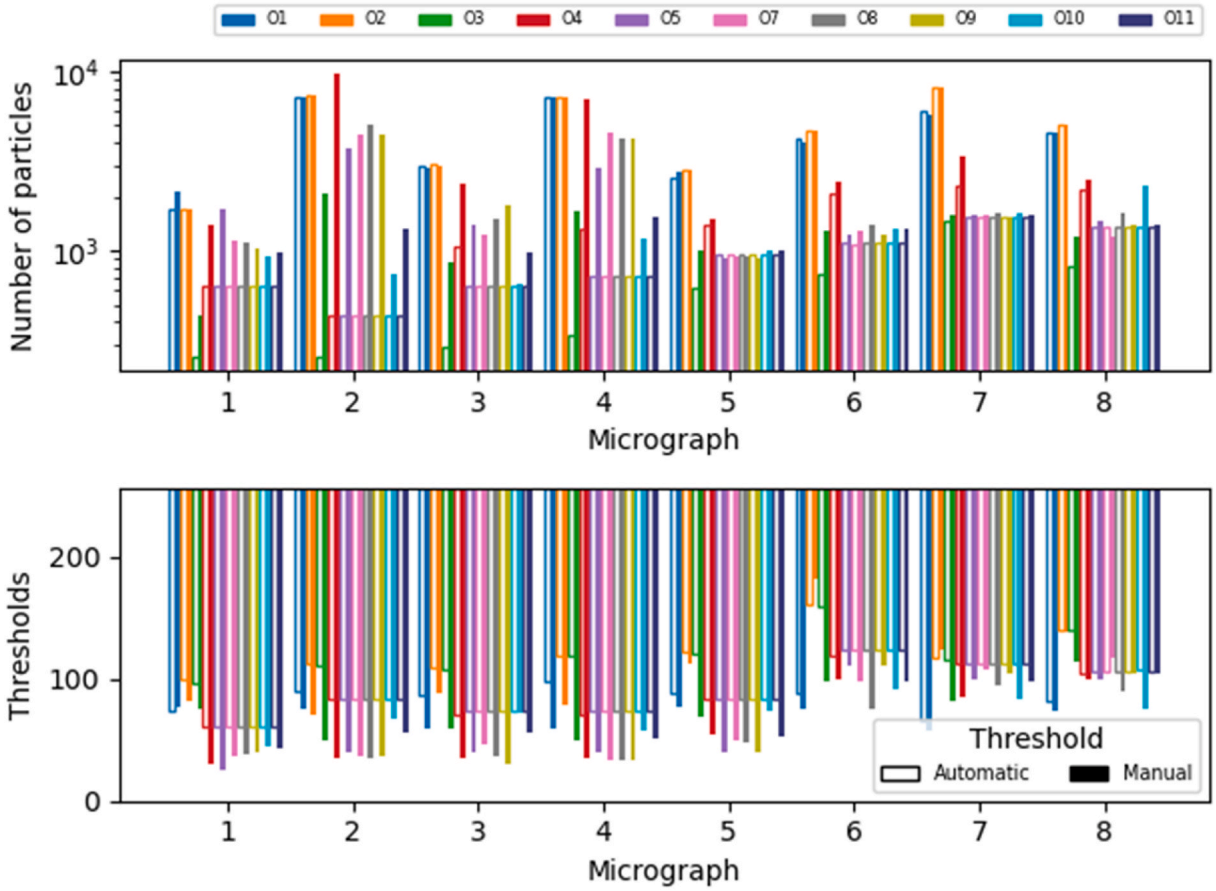

Fig. 8. Number of particles and the upper and lower thresholds set by ImageJ (for Automatic), or manually by each operator. This is displayed for micrographs 01 to 08. The legend at the top indicates the operator number (each assigned a color).

The bars are filled to indicate when the manual threshold approach was used and are unfilled for the automatic approach. In 79% of the cases, the human operator has chosen lower thresholds than the automatic ones. Lower thresholds increase the number of detected particles. This means that a human operator tends to favor more particles than an ImageJ automatic algorithm; the median value is 60% more particles. But, in some cases, there can be a factor as high as 20 between the number of particles for the manual and the automatic methods.

The operators that generate the greatest number of exceptions to this trend are O1 and O2. For these, an automatic threshold was found to be lower than the manual threshold in 75% of the micrographs. For the other operators, exceptions were found in less than 25% of the micrographs. Four operators had no exceptions.

Regarding the automatic thresholding procedure, care needs to be taken when using ImageJ as the software of choice. During the project, it became clear that several different ways of auto thresholding are available in ImageJ. Two examples are noteworthy, applied via the menu sequences: (a) Image ⟩ Adjust ⟩ Auto Threshold, or (b) Image ⟩ Adjust ⟩ Threshold [51]. There is evidence that Auto Threshold (a) is part of Fiji, and not a core part of ImageJ. While the Auto Threshold plugin (a) can use or ignore the extremes of the image histogram (Ignore black, Ignore white), Threshold (b) cannot; the "Default" option in Threshold (b) ignores the histogram extremes, but the other methods (e.g. Triangle, Otsu, IsoData, etc.) do not. This means that applying the two commands to the same image can apparently produce different results. This was observed and verified during the round-robin study. In essence, the Auto Threshold plugin (a), with the correct settings, can reproduce the results of the Threshold (b), but not the other way around. Image ⟩ Adjust ⟩ Threshold (followed by Default and Dark background) is noteworthy in that this was used by O4 through O11 in the round-robin (Please refer to

Table 3). This generates setAutoThreshold("Default dark") when the Record feature is utilized in ImageJ. Another operator (O3) utilized the Auto Threshold plugin (a). It was confirmed that the use of the latter for the threshold settings reduces the number of particles counted and thus the fractional area coverage compared to the Threshold (b) sequence.

Looking at the results of the study, some differences in particle detection can be noticed that are likely to depend on the adopted methodology. Operators O1 and O2 used a variant of Image 〉 Adjust 〉 Threshold in which Dark and "Otsu" and/or "Triangle" were selected from the pop-up box. They also used sophisticated masking techniques. Looking at several of the micrographs and a binarized image, it was noticed that Threshold (b) plus Default detects fewer small particles than using the procedures of O1 and O2. Considering this same aspect, it was noticed that when manually setting the threshold, O4–O11 increased the range of thresholding values to detect and register a higher number of smaller particles. Interestingly, the number of particles detected by O4–O11 tended to be closer to the results of O1 and O2 for most of the low-soiling samples (micrographs 1–4). Regarding the differences in default auto thresholding techniques, without adequate guidelines or a suitable reference image, it is difficult to say which is "true" as long as all visible particles in the image are pre-processed to allow for detection using various auto thresholding techniques. An attempt to find a meaningful correlation between the number of particles and the thresholding levels using the results in Fig. 8 was not successful.

This raises the question as to which threshold is correct. According the ImageJ wiki community [52], it is not easy to extract the necessary data from an image. They write, "It will always be, to some extent, in the eye of the user/observer/scientist and will also be impacted by empirically collected knowledge. The basic problem of deciding if a threshold (or in general an extraction method) is 'good' needs a 'ground truth'. But such a ground truth is not naturally existing, and is always created in one or the other way by a human. So, describing which method you use - and/or showing a comparison with other methods - is probably the best you can do to enable a statement on the quality of the extraction."

Referring to Table 3, we can also consider the exclusion of particles that are cut off by the edge or perimeter of the micrograph. Again, there are no clear guidelines; they appear to matter, so they are worthy of some discussion in cases where their relevance may depend on the goal of the analysis. To retrieve an accurate particle size distribution (PSD) from a micrograph, the analysis should exclude incomplete particles, since their size is indeterminate. If the ratio of detected particles that intersect with the boundaries of the micrographs is not negligible, the additional command option "exclude" for the particle analysis procedure should be used. Then, diameter and other geometrical measurements are only performed on particles that are seen entirely. But for the fractional area coverage, the results should be included to better assess the area coverage of the soiled sample, which directly connects to the power loss in a PV or CSP solar conversion system.

3.5. Lessons learnt, recommendations and additional sources of uncertainty

The results of the present work highlight an issue that has been thus far neglected by the PV and CSP soiling communities. Over the years, many researchers have been using image analysis to characterize outdoor soiling at different locations. However, so far, the reliability and variance of the image analysis results has not been questioned. The present analysis raises a concern on the use of this technique. As shown, even if the same micrograph is analysed using the same software, significantly dissimilar results can be found.

It was mentioned that several authors successfully correlated surface area coverage to transmittance [10–15]. However, a previous work already highlighted dissimilarities among those correlations [22], possibly also due to factors such as dust type. The results of the present work confirm that if one wants to use these types of correlations, all data points have to be consistently analysed. It has been shown in the present study that particle coverage results might change depending on the image analysis process. The fractional area coverage returns median coefficients of variation of 35% (top portion of Fig. 7). This possibly explains, at least in part, the variability in the previously reported correlations. Therefore, in lieu of a standard methodology or guidelines, correlations in the literature should not be expected to work for all soiling datasets. It is also recommended that any image analysis methodologies be well-documented and reported in a detailed fashion. Specific and quantitative analyses performed by one laboratory should not *a priori* be viewed as transferable to another. For the moment, and with caution, only qualitative and general trends can be made. Cross checking and revalidation of any correlations are thus recommended when a new set of data is processed.

On the other hand, however, ImageJ was found not to introduce any stochastic variation in the results, at least for the methodologies employed in this work. In order to prove this assertion, the methodologies of O1, O2, and O5 were indeed applied multiple times on the same figures. No difference was found among the results of the different iterations when the same method was repeatedly applied to the same micrograph (For details, please refer to the Supplemental Information and Mendeley data archive.).

The main focus of this work has been the evaluation of the precision of image analysis. Indeed, as previously pointed out, an assessment of accuracy would require the use of a reference image, where the particle number and the diameter were already known. However, this was not available at the time this round robin was conducted. The assessment of the accuracy of the various methodologies should be the focus of future studies, which should contribute to the development of recommendations and an industry standard for the image analysis of PV and CSP soiling.

Future works should also enhance some aspects of the present study, adding more parameters to the analysis. The number of micrographs should be increased as well. This way, the impact of the lighting, the magnification and the type of microscope could also be differentiated. Indeed, each of the aforementioned empirical correlations were obtained through different campaigns, equipment and image analysis methodologies [10–15]. In the present case, the investigated micrographs were taken during a single soiling collection campaign, utilizing the same microscope in dark field mode at a fixed magnification. However, different campaigns might make use of different microscopes, settings and/or set-ups. This means that the variability in the soiling characterization should not be solely attributed to the image analysis process. Indeed, the sequence of events for obtaining particle characterization analysis are (in order): sample soiling, sample transportation, microscope set up (including illumination), image capture and image analysis using software tools such as ImageJ. Each of these steps can introduce additional uncertainty in the soiling characterization process and, for this reason, should be taken into account in future studies. Moreover, there are admittedly other sources of variation in the image analysis for the assessment and characterization of soiling. These would include the variance due to non-uniformities in soiling across the glass coupon (samples) [53]. These variabilities and uncertainties should also be the topic of future work. All these variabilities, in addition to the lack of standardized image processing methods, make it impossible at the present time to recommend a universal micrograph analysis methodology, as the type of soiling, the experimental procedure and the microscope set up can affect the output of the various methodologies.

4. Conclusions

Soiling in both PV and CSP systems reduces the yield of energy from the sun. If progress is to be made regarding anti-soiling coatings, cleaning methods and mitigation techniques, there needs to be an understanding of the correlation between the output of the solar conversion system, its transmission losses and the microscopic properties of the deposited particles (i.e., particle size distribution and fractional area

coverage). For the latter, the readily available image analysis tools yield different results depending upon operator and the analysis method. It is, however, possible to understand the uncertainty of the analysis and to select parameters that are closer to invariant with respect to operator and method. This work presents the results from an international round-robin study in which various experts utilized automatic and manual methods to characterize soiling using the image analysis software ImageJ. While the coefficient of variation of the fractional area coverage was found to be approximately 35%, the value for the mean particle size was approximately 15% and the value for number of particles could be over 80%.

The results of the present work led to two main conclusions. First, due to a lack of a standard methodology and a suitable reference image, the image analysis is subject to significant uncertainty. The results of micrograph-based soiling characterization can vary depending on the operator, even if the same image and the same processing software are employed. Furthermore, a particular image analysis procedure might give a reasonable variability for one micrograph, but may give a larger variability for another. The required procedure may need to be modified. The second conclusion, however, is that it was found that some parameters are less variable than others, and therefore more robust to image analysis. This opens the possibility to the discovery of other parameters that would be useful for comparing results across various laboratories and studies. In addition, when the same procedures were used multiple times, the same results were generated. In other words, ImageJ does not intrinsically induce a stochastic variation when the methods presented in this work are employed.

ImageJ was employed in this work because of its dominance in particle analysis studies, and because it is familiar to the soiling community. However, alternative software packages are available and could introduce additional variabilities. Also, it should be also highlighted that the present analysis focused on a single set of micrographs of soiling collected at various locations, but which were taken using the same technique and the same microscope by one microscopist. This means that, in addition to the uncertainty due to the particle analysis procedure, additional uncertainty could be introduced by other factors not taken into account, such as the use of a different magnification factor, different microscopes and different lighting. Experimental campaigns can indeed rely on dissimilar protocols, which can introduce additional uncertainties. Therefore, additional studies and round robins are needed to evaluate the robustness of the present findings and to expand them to different conditions. Because of the variety of variables involved in recording a micrograph, one could expect that different procedures might be required for different sets of micrographs. All these issues should be addressed in future works.

It is also recommended that a detailed description of image analysis methodologies be reported when they are used in soiling characterization studies. When comparing soiling results from microscopy across different studies and laboratories, only qualitative and general trends are reliable. For quantitative analyses, error bars similar to those presented in this round-robin study can be considered. Since one of the central tenets of the scientific method is to agree on standard procedures and to understand their uncertainty, this study lays groundwork for better collaboration and concerted efforts towards improving the performance of all solar energy conversion systems.

CRediT authorship contribution statement

Greg P. Smestad: Writing – original draft, Visualization, Validation, Methodology, Investigation, Formal analysis, Conceptualization. **Cody Anderson:** Writing – review & editing, Validation, Investigation, Formal analysis. **Michael E. Cholette:** Writing – review & editing, Supervision. **Pavan Fuke:** Writing – review & editing, Investigation, Formal analysis. **Ahmed Amine Hachicha:** Writing – review & editing, Investigation, Formal analysis. **Anil Kottantharayil:** Writing – review & editing, Supervision. **Klemens Ilse:** Writing – review & editing, Investigation, Data curation, Conceptualization. **Mounia Karim:** Writing – review & editing, Investigation, Formal analysis. **Muhammad Zahid Khan:** Writing – review & editing, Investigation, Formal analysis, Data curation. **Herbert Merkle:** Writing – review & editing, Investigation, Formal analysis. **David C. Miller:** Writing – review & editing, Investigation. **Jimmy M. Newkirk:** Writing – review & editing, Investigation, Formal analysis. **Giovanni Picotti:** Writing – review & editing, Supervision. **Florian Wiesinger:** Writing – review & editing, Validation, Investigation, Formal analysis. **Guido Willers:** Writing – review & editing, Investigation, Formal analysis. **Leonardo Micheli:** Writing – original draft, Visualization, Validation, Software, Methodology, Formal analysis, Conceptualization.

Declaration of competing interest

The authors declare no conflicts of interest. The views expressed in the article do not necessarily represent the views of the DOE or the U.S. Government. Instruments and materials are identified in this paper to describe the experiments. In no case does such identification imply recommendation or endorsement by NREL. The U.S. government retains and the publisher, by accepting the article for publication, acknowledges that the U.S. Government retains a nonexclusive, paid-up, irrevocable, worldwide license to publish or reproduce the published form of this work, or allow others to do so, for U.S. Government purposes.

Data availability

The data and the ImageJ macros are available on a Mendeley Archive https://doi.org/10.17632/sss2jf7t9g.1.

Acknowledgements

Cody Anderson, Giovanni Picotti, and Michael Cholette acknowledge the support of the Australian Renewable Energy Agency (ARENA), within the framework of the Australian Solar Thermal Research Institute (ASTRI – Project P54). Ahmed Amine Hachicha would like to thank the University of Sharjah, Project # 20020406150, for its financial support. This work was co-authored by the National Renewable Energy Laboratory, operated by Alliance for Sustainable Energy, LLC, for the U.S. Department of Energy (DOE) under Contract No. DE-AC36-08GO28308 and agreement number 38263. Pavan Sunil Fuke and Anil Kottantharayil would like to acknowledge the Ministry of New and Renewable Energy of the Government of India for supporting their work through the National Centre for Photovoltaic Research and Education (NCPRE) at IIT Bombay through the Project No. No. 313-21/11/2022- Solar R&D. Pavan Fuke also acknowledges the Prime Minister Research Fellowship (PMRF) program for financial support. Florian Wiesinger (DLR) received funding from the European Union's Horizon 2020 Research and Innovation Action (RIA) COMPASsCO_2 under grant agreement No. 958418. Leonardo Micheli was supported by Sole4PV, a project funded by the Italian Ministry of University and Research under the 2019 «Rita Levi Montalcini » Program for Young Researchers.

The authors would like to thank the following people and institutions for the soiled glass samples utilized in this round-robin study: Prof. Dr. Jorge Rabanal-Arabach (Centro de Desarrollo Energético Antofagasta, Universidad de Antofagasta, Chile) and the Center for Energy Development Antofagasta (CDEA). The authors acknowledge those entities and institutions, as well as the support of the Chilean Economic Development Agency (CORFO) under contract No 17PTECES-75830 under the framework of project "AtaMoS TeC."The soiled samples from the Atacama Desert were collected on the Plataforma Solar de Antofagasta (PSDA) test site of the CDEA;Dr. Said Bentouba (University of Adrar, currently at the NORCE Norwegian Research Centre) and the University of Adrar, Algeria; Prof. Dr. Ahmed Alami Merrouni (now at the Mohamed First University, Oujda, Morocco) and the Green Energy Park, Recherche en Energie Solaire et Energies Nouvelles (IRESEN), as well as

the Mohammed VI Polytechnic University in Ben Guerir; Paul Rodden, Ekistica and the Desert Knowledge Australia Solar Centre (DKASC); Dr. Brahim Aissa and Benjamin W. Figgis of the Qatar Environment and Energy Research Institute (QEERI) Outdoor Test Facility of the Hamad Bin Khalifa University; Ryo Huntamer (now of Philips, San Diego), Prof. Alfredo A. Martinez-Morales and University of California, Riverside Bourns College of Engineering Center for Environmental Research and Technology (CE-CERT), Southern California Research Initiative for Solar Energy (SC-RISE). This research was partially supported by a grant from UC Solar (MR-15-328386); Dr. Thomas Müller, the Leibniz Institute for Tropospheric Research (TROPOS) and the Cape Verde Atmospheric Observatory (CVAO); Yanal Alamat HTWK Leipzig, currently at INROS LACKNER SE Hamburg), Prof. Dr. Winfried Hähle and the Hochschule für Technik, Wirtschaft und Kultur, Leipzig (HTWK Leipzig) for providing the soiled glass samples from Amman, Jordan. The guidance and fruitful discussions with Katja Lange of the Fraunhofer CSP are gratefully acknowledged.

Appendix A. Supplementary data

Supplementary data to this article can be found online at https://doi.org/10.1016/j.solmat.2023.112437.

References

[1] Department of Economic, Social Affairs, The Sustainable Development Goals Report, 2016, https://doi.org/10.1177/000331979004100307. New York, NY.
[2] SolarPower Europe, Global Market Outlook for Solar Power 2022-2026, 2022.
[3] M.T. Islam, N. Huda, A.B. Abdullah, R. Saidur, A comprehensive review of state-of-the-art concentrating solar power (CSP) technologies: current status and research trends, Renew. Sustain. Energy Rev. 91 (2018) 987–1018, https://doi.org/10.1016/j.rser.2018.04.097.
[4] R. Conceição, J. González-Aguilar, A.A. Merrouni, M. Romero, Soiling effect in solar energy conversion systems: a review, Renew. Sustain. Energy Rev. 162 (2022), https://doi.org/10.1016/j.rser.2022.112434.
[5] K. Ilse, M.Z. Khan, N. Voicu, V. Naumann, C. Hagendorf, J. Bagdahn, Advanced performance testing of anti-soiling coatings – Part I: sequential laboratory test methodology covering the physics of natural soiling processes, Sol. Energy Mater. Sol. Cells 202 (2019), 110048, https://doi.org/10.1016/j.solmat.2019.110048.
[6] R.K. Jones, A. Baras, A. Al Saeeri, A. Al Qahtani, A.O. Al Amoudi, Y. Al Shaya, M. Alodan, S.A. Al-Hsaien, Optimized cleaning cost and schedule based on observed soiling conditions for photovoltaic plants in Central Saudi Arabia, IEEE J. Photovoltaics 6 (2016) 730–738, https://doi.org/10.1109/JPHOTOV.2016.2535308.
[7] G. Picotti, L. Moretti, M.E. Cholette, M. Binotti, R. Simonetti, E. Martelli, T. A. Steinberg, G. Manzolini, Optimization of cleaning strategies for heliostat fields in solar tower plants, Sol. Energy 204 (2020) 501–514, https://doi.org/10.1016/j.solener.2020.04.032.
[8] International Electrotechnical Commission, Photovoltaic System Performance – Part 1: Monitoring, IEC 61724-1, Edition 1.0, 2017-03, 2017.
[9] M. Valerino, M. Bergin, C. Ghoroi, A. Ratnaparkhi, G.P. Smestad, Low-cost solar PV soiling sensor validation and size resolved soiling impacts: a comprehensive field study in Western India, Sol. Energy 204 (2020) 307–315, https://doi.org/10.1016/j.solener.2020.03.118.
[10] B. Figgis, A. Ennaoui, B. Guo, W. Javed, E. Chen, Outdoor soiling microscope for measuring particle deposition and resuspension, Sol. Energy 137 (2016) 158–164, https://doi.org/10.1016/j.solener.2016.08.015.
[11] M.A. Bahattab, I.A. Alhomoudi, M.I. Alhussaini, M. Mirza, J. Hegmann, W. Glaubitt, P. Löbmann, Anti-soiling surfaces for PV applications prepared by sol-gel processing: comparison of laboratory testing and outdoor exposure, Sol. Energy Mater. Sol. Cells 157 (2016) 422–428, https://doi.org/10.1016/j.solmat.2016.07.004.
[12] P.D. Burton, A. Hendrickson, S.S. Ulibarri, D. Riley, W.E. Boyson, B.H. King, Pattern effects of soil on photovoltaic surfaces, IEEE J. Photovoltaics 6 (2016) 976–980, https://doi.org/10.1109/JPHOTOV.2016.2567100.
[13] K.K. Ilse, B.W. Figgis, M. Werner, V. Naumann, C. Hagendorf, H. Pöllmann, J. Bagdahn, Comprehensive analysis of soiling and cementation processes on PV modules in Qatar, Sol. Energy Mater. Sol. Cells 186 (2018) 309–323, https://doi.org/10.1016/j.solmat.2018.06.051.
[14] G.P. Smestad, T.A. Germer, H. Alrashidi, E.F. Fernández, S. Dey, H. Brahma, N. Sarmah, A. Ghosh, N. Sellami, I.A.I.A.I. Hassan, M. Desouky, A. Kasry, B. Pesala, S. Sundaram, F. Almonacid, K.S.S. Reddy, T.K. Mallick, L. Micheli, Modelling photovoltaic soiling losses through optical characterization, Sci. Rep. 10 (2020) 58, https://doi.org/10.1038/s41598-019-56868-z.
[15] A. Einhorn, L. Micheli, D.C. Miller, L.J. Simpson, H.R. Moutinho, B. To, C. L. Lanaghan, M.T. Muller, S. Toth, J.J. John, S. Warade, A. Kottantharayil, C. Engtrakul, Evaluation of soiling and potential mitigation approaches on photovoltaic glass, IEEE J. Photovoltaics 9 (2019) 233–239, https://doi.org/10.1109/JPHOTOV.2018.2878286.
[16] A.A. Hachicha, I. Al-Sawafta, Z. Said, Impact of dust on the performance of solar photovoltaic (PV) systems under United Arab Emirates weather conditions, Renew. Energy 141 (2019) 287–297, https://doi.org/10.1016/j.renene.2019.04.004.
[17] P.D. Burton, B.H. King, Application and characterization of an artificial grime for photovoltaic soiling studies, IEEE J. Photovoltaics 4 (2014) 299–303.
[18] G. Picotti, R. Simonetti, T. Schmidt, M.E. Cholette, A. Heimsath, S.J. Ernst, G. Manzolini, Evaluation of reflectance measurement techniques for artificially soiled solar reflectors: experimental campaign and model assessment, Sol. Energy Mater. Sol. Cells 231 (2021), 111321, https://doi.org/10.1016/j.solmat.2021.111321.
[19] A. Mazzoli, O. Favoni, Particle size, size distribution and morphological evaluation of airborne dust particles of diverse woods by Scanning Electron Microscopy and image processing program, Powder Technol. 225 (2012) 65–71, https://doi.org/10.1016/j.powtec.2012.03.033.
[20] Y.Y. Quan, L.Z. Zhang, Experimental investigation of the anti-dust effect of transparent hydrophobic coatings applied for solar cell covering glass, Sol. Energy Mater. Sol. Cells 160 (2017) 382–389, https://doi.org/10.1016/j.solmat.2016.10.043.
[21] L. zhi Zhang, A. jian Pan, R. rong Cai, H. Lu, Indoor experiments of dust deposition reduction on solar cell covering glass by transparent super-hydrophobic coating with different tilt angles, Sol. Energy 188 (2019) 1146–1155, https://doi.org/10.1016/j.solener.2019.07.026.
[22] J.G. Bessa, L. Micheli, F. Almonacid, E.F. Fernández, Monitoring photovoltaic soiling: assessment, challenges, and perspectives of current and potential strategies, iScience 24 (2021), 102165, https://doi.org/10.1016/j.isci.2021.102165.
[23] H. Qasem, T.R. Betts, H. Müllejans, H. AlBusairi, R. Gottschalg, Dust-induced shading on photovoltaic modules, Prog. Photovoltaics Res. Appl. 22 (2014) 218–226, https://doi.org/10.1002/pip.2230.
[24] Global Modeling and Assimilation Office (GMAO), MERRA-2 tavg1_2d_slv_Nx: 2d,1-Hourly,Time-Averaged,Single-Level,Assimilation, Single-Level Diagnostics V5 12 (4) (2019), https://doi.org/10.5067/VJAFPLI1CSIV.
[25] Global Modeling and Assimilation Office (GMAO), MERRA-2 tavg1_2d_aer_Nx: 2d,1-Hourly,Time-averaged,Single-Level,Assimilation,Aerosol Diagnostics 0.625 x 0.5 degree V5.12.4 (M2T1NXAER), (n.d.). https://doi.org/10.5067/KLICLTZ8EM9D.
[26] M.C. Peel, B.L. Finlayson, T.A. McMahon, Updated world map of the Köppen-Geiger climate classification, Hydrol. Earth Syst. Sci. 11 (2007) 1633–1644, https://doi.org/10.5194/hess-11-1633-2007.
[27] C.A. Schneider, W.S. Rasband, K.W. Eliceiri, NIH Image to ImageJ: 25 years of image analysis, Nat. Methods 9 (2012) 671–675, https://doi.org/10.1038/nmeth.2089.
[28] J. Schindelin, I. Arganda-Carreras, E. Frise, V. Kaynig, M. Longair, T. Pietzsch, S. Preibisch, C. Rueden, S. Saalfeld, B. Schmid, J.-Y. Tinevez, D.J. White, V. Hartenstein, K. Eliceiri, P. Tomancak, A. Cardona, Fiji: an open-source platform for biological-image analysis, Nat. Methods 9 (2012) 676–682, https://doi.org/10.1038/nmeth.2019.
[29] K.K. Ilse, J. Rabanal, L. Schonleber, M.Z. Khan, V. Naumann, C. Hagendorf, J. Bagdahn, Comparing indoor and outdoor soiling experiments for different glass coatings and microstructural analysis of particle caking processes, IEEE J. Photovoltaics 8 (2017) 203–209, https://doi.org/10.1109/JPHOTOV.2017.2775439.
[30] D. Olivares, P. Ferrada, A. Marzo, J. Llanos, C. Miranda-Ostojic, V. del Campo, S. Bravo, E. Fuentealba, Microstructural analysis of the PV module cementation process at the solar platform of the Atacama Desert, Sol. Energy Mater. Sol. Cells 227 (2021), 111109, https://doi.org/10.1016/j.solmat.2021.111109.
[31] B. Figgis, B. Guo, W. Javed, S. Ahzi, Y. Rémond, Dominant environmental parameters for dust deposition and resuspension in desert climates, Aerosol Sci. Technol. 52 (2018) 788–798, https://doi.org/10.1080/02786826.2018.1462473.
[32] R. Conceição, H. Silva, J. Mirão, M. Collares-Pereira, Organic soiling: the role of pollen in PV module performance degradation, Energies 11 (2018) 294, https://doi.org/10.3390/en11020294.
[33] K. Ilse, B. Figgis, M.Z. Khan, V. Naumann, C. Hagendorf, Dew as a detrimental influencing factor for soiling of PV modules, IEEE J. Photovoltaics 9 (2019) 287–294, https://doi.org/10.1109/JPHOTOV.2018.2882649.
[34] S. Sengupta, S. Sengupta, H. Saha, Comprehensive modeling of dust accumulation on PV modules through dry deposition processes, IEEE J. Photovoltaics 10 (2020) 1148–1157, https://doi.org/10.1109/JPHOTOV.2020.2992352.
[35] A. Roslizar, J. Taddeucci, U. Paetzold, H. Holscher, B. Richards, Influence of wind speed on volcano ash removal from self-cleaning cover films dedicated for photovoltaics, IEEE J. Photovoltaics 12 (2022) 453–460, https://doi.org/10.1109/JPHOTOV.2021.3117913.
[36] International Organization for Standardization (ISO), ISO 13322-1:2014 Particle Size Analysis — Image Analysis Methods — Part 1: Static Image Analysis Methods, 2014.
[37] International Organization for Standardization (ISO), ISO 9276-1:1998 Representation of Results of Particle Size Analysis — Part 1: Graphical Representation, 2020.
[38] International Organization for Standardization (ISO), ISO 9276-2:2014 Representation of Results of Particle Size Analysis — Part 2: Calculation of Average Particle Sizes/diameters and Moments from Particle Size Distributions, 2019.
[39] NIST/SEMATECH, E-Handbook of Statistical Methods, (n.d.). https://doi.org/doi.org/10.18434/M32189.

[40] Institute of Environmental Sciences and Technology, IEST-STD-CC1246E, Product Cleanliness Levels – Applications, Requirements, and Determination, 2013.
[41] W.C. Krumbein, Size frequency distributions of sediments, SEPM J. Sediment. Res. 4 (1934), https://doi.org/10.1306/d4268eb9-2b26-11d7-8648000102c1865d.
[42] International Standards Organization, ISO 14688-1: Geotechnical Investigation and Testing — Identification and Classification of Soil — Part 1, Identification and description, Geneva, Switzerland, 2017.
[43] ASTM International, ASTM E691-21 Standard Practice for Conducting an Interlaboratory Study to Determine the Precision of a Test Method, 2021, https://doi.org/10.1520/E0691-21.
[44] E. Jones, E. Oliphant, P. Peterson, et al., SciPy: Open Source Scientific Tools for Python, 2001. http://www.scipy.org/.
[45] I. Nayshevsky, Q. Xu, A. Lyons, Literature survey of dust particle dimensions on soiled solar panel modules, 2018, Int. PV Soiling Work (2018), 62788.
[46] P. Bellmann, F. Wolfertstetter, R. Conceição, H.G. Silva, Comparative modeling of optical soiling losses for CSP and PV energy systems, Sol. Energy 197 (2020) 229–237, https://doi.org/10.1016/j.solener.2019.12.045.
[47] C. Sanz-Saiz, J. Polo, N. Martín-Chivelet, M. del C. Alonso-García, Soiling loss characterization for Photovoltaics in buildings: a systematic analysis for the Madrid region, J. Clean. Prod. 332 (2022), 130041, https://doi.org/10.1016/j.jclepro.2021.130041.
[48] R. Conceição, H.G. Silva, J. Mirão, M. Gostein, L. Fialho, L. Narvarte, M. Collares-Pereira, Saharan dust transport to Europe and its impact on photovoltaic performance: a case study of soiling in Portugal, Sol. Energy 160 (2018) 94–102, https://doi.org/10.1016/j.solener.2017.11.059.
[49] P.D. Burton, L. Boyle, J.J.M. Griego, B.H. King, Quantification of a minimum detectable soiling level to affect photovoltaic devices by natural and simulated soils, IEEE J. Photovoltaics 5 (2015) 1143–1149, https://doi.org/10.1109/JPHOTOV.2015.2432459.
[50] M. Krzywinski, N. Altman, Points of significance: error bars, Nat. Methods 10 (2013) 921–922, https://doi.org/10.1038/nmeth.2659.
[51] Imagej.net, Auto Threshold, 2023. https://imagej.net/plugins/auto-threshold. (Accessed 3 March 2023).
[52] Imagej.net, Thresholding, 2023. https://imagej.net/imaging/thresholding. (Accessed 23 May 2023).
[53] I.S. Khan, J. Morse, R.R. White, D.C. Miller, A custom high-throughput optical mapping instrument for accelerated stress testing of PV module materials, IEEE J. Photovoltaics 12 (2022) 73–80, https://doi.org/10.1109/JPHOTOV.2021.3122925.

https://dspace.org/

Variability and associated uncertainty in image analysis for soiling characterization in solar energy systems

Smestad, Greg P.; Anderson, Cody; Cholette, Michael E.; Fuke, Pavan; Hachicha, Ahmed Amine ...

2023-08-15
Elsevier
https://doi.org/10.1016/j.solmat.2023.112437
Smestad GP, Anderson C, Cholette ME, et al., (2023) Variability and associated uncertainty in image analysis for soiling characterization in solar energy systems. Solar Energy Materials and Solar Cells, Volume 259, August 2023, Article number 112437

Downloaded from a DSpace repository. https://dspace.org/